Supporting Information

Developing Quantitative Non-Destructive Characterization of Nanomaterials: Case Study on Sequential Infiltration Synthesis of Block Copolymers

Eleonora Cara,1* Philipp Hönicke,2 Yves Kayser,2†
Jörg K. N. Lindner,3 Micaela Castellino4, Irdi Murataj,1-4 Samuele Porro,4 Angelo Angelini,1 Natascia De Leo,1 Candido Fabrizio Pirri,4 Burkhard Beckhoff,2 Luca Boarino1, Federico Ferrarese Lupi1*

[1] *Advanced Materials and Life Science Division, Istituto Nazionale Ricerca Metrologica (INRiM), Strada delle Cacce 91, 10135 Torino, Italy*

[2] *Physikalisch-Technische Bundesanstalt (PTB), Abbestr. 2-12, 10587 Berlin, Germany*

[3] *AG Nanostrukturierung, Nanoanalyse und Photonische Materialien, Paderborn University , Warburger Str. 100, 33098 Paderborn, Germany*

[4] *Dipartimento di Scienza Applicata e Tecnologia, Politecnico di Torino, Corso Duca degli Abruzzi, 24, Torino, Italy*

† Max Planck Institute for Chemical Energy Conversion, Stiftstr. 34-36, 45470 Mülheim an der Ruhr, Germany

Corresponding authors' emails*: f.ferrareselupi@inrim.it, e.cara@inrim.it

GIXRF characterization

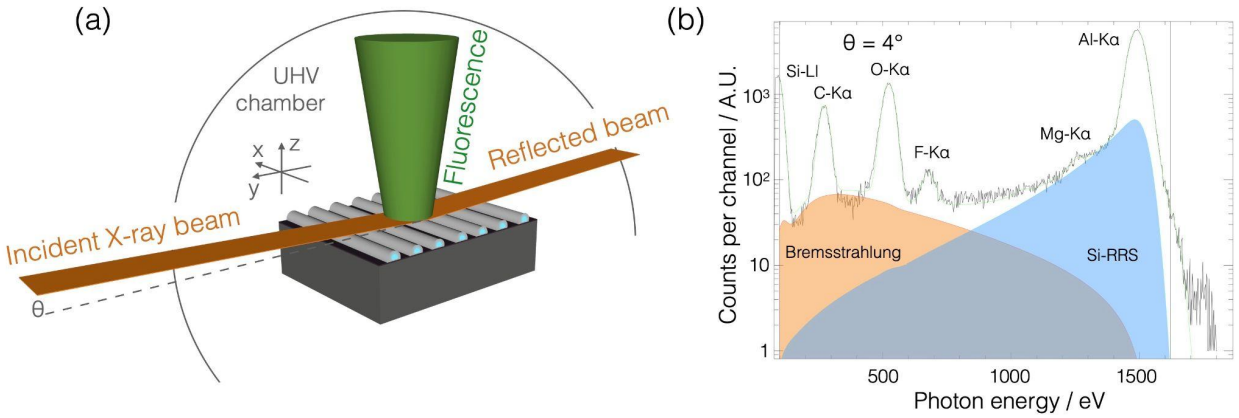

Figure S1. (a) Schematic illustration of the GIXRF measurement configuration on the infiltrated samples inserted in a UHV chamber and mounted on a motorized stage where displacement along x, y, and z axes is modified as well as the sample inclination θ with respect to the incident beam. The elemental components of the sample are excited to fluorescence by a monochromatic X-ray beam at 1.622 keV which impinges on the sample surface at a grazing angle θ from 0° to 7°. The fluorescent radiation is emitted in a cone-shaped region and detected perpendicularly to the sample surface. Below the critical angle for total external reflection, ~1° the beam is completely reflected, symmetrically to the incident one. (b) The fluorescence spectrum was acquired at incident angle θ = 4° on the PMMA10 sample. The continuous Bremsstrahlung and resonant Raman scattering contributions are included in the deconvolution procedure and colored in orange and light blue, respectively. The Al-Kα,β, and C-Kα fluorescence peaks in the XRF spectra are integrated at each angle.

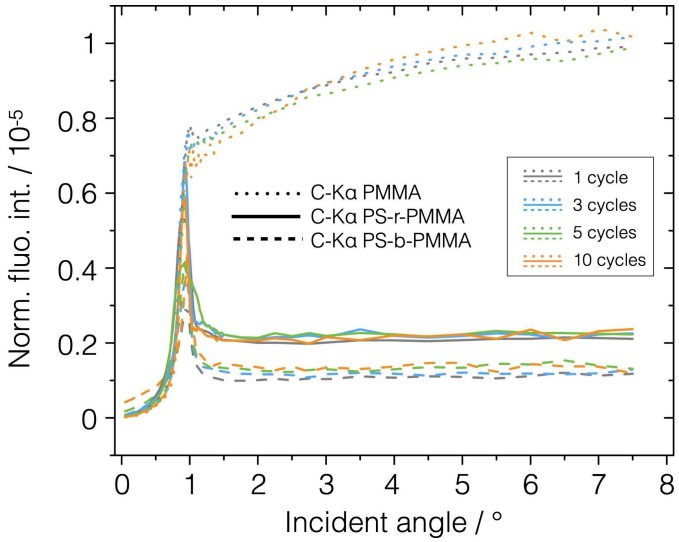

Figure S2. The angular profiles corresponding to C-Kα fluorescence lines, extracted from the three polymeric sample sets, are shown with dotted lines for PMMA, solid lines for RCP, and dashed lines for BCP samples. The color code is referred to the number of ALD cycles. In the angular range suitable for quantification of the mass per unit area (above 2°), the average intensity remains constant for PMMA and RCP samples treated with different numbers of cycles. On the other hand, the average intensity for BCP samples has a relative increase of approximately 30 % from 1 to 10 cycles, as shown in the scatter plot in Figure 3a.

Homogeneity of the infiltration process

The GIXRF characterization is performed through the employment of physically calibrated instrumentation. This allows considering all the uncertainty contributions to the determination of the metallic mass per unit area. The uncertainties reported in the scatter plot in Figure 2a are mainly given by the estimated relative uncertainty of 10 % on the fluorescence yield $\omega_{Al,K}$, and 5 % on the partial photoionization cross-section. The determination of the effective solid angle of detection introduces a 4 % contribution to the uncertainty budget while other instrumental parameters contribute with 2 %. Moreover, a relative uncertainty of 1.5 % can be considered due to the determination of Al count rates by the spectral deconvolution and 2.5% is introduced by the Al counting statistics. The relative uncertainties are propagated by the root sum of squares of all contributions giving a total of 12.3%.

The homogeneity of the Al areal density was evaluated over a large area by carrying out a scan measurement along the width of the sample (y-axis) at a fixed angle of incidence equal to the maximum of the θ-scan (7.5°). The scan was performed over a distance of 8-10 mm for each sample. The scatter plots in Figure S3a,b,c,d show the mass per unit area as a function of the absolute motor position along the y-axis of the sample for native oxide samples, BCP, RCP, and PMMA samples, respectively. The Al areal density was found to be constant within the error bars indicating a good homogeneity of the ALD-SIS process. Some discrepancies from the average value are found at the edge of the scanning interval in the y direction which might correspond to the edge of the substrate where the deposition of the polymeric layer by spin coating can present some inhomogeneities.

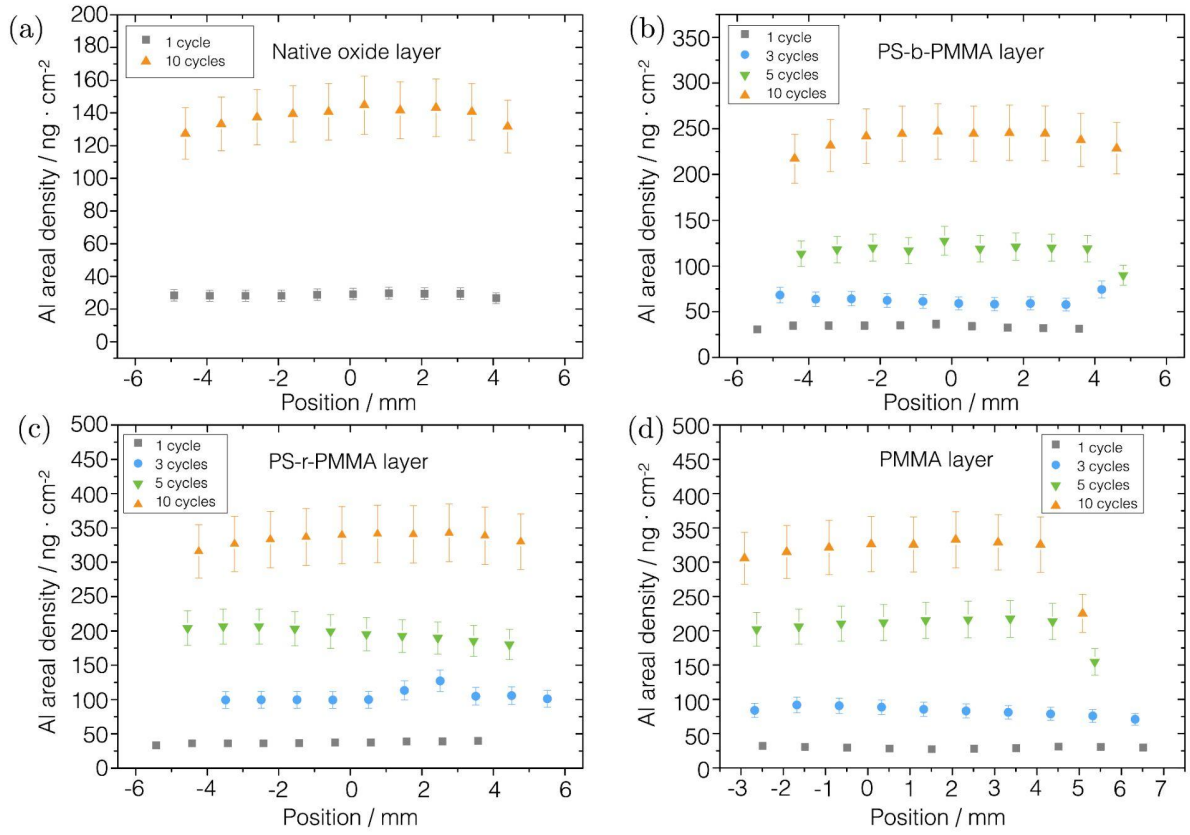

Figure S3. Scatter plots reporting the Al mass per unit area for different ALD processes as a function of the absolute motor position along the width of the (a) Si/SiO_2 samples, (b) PS-*b*-PMMA layer samples, (c) PS-*r*-PMMA layer samples, and (d) PMMA layer samples.

XPS depth profiling

The depth profile is obtained for each sample by extracting the intensity of the signal for the elements of interest from the XPS spectrum acquired after each etching step. Figure S4a reports, as an example, the 100 spectra acquired after as many etching steps every $\Delta t = 0.1$ min on the sample PMMA10. The same holds for the other analyzed samples BCP10 and RCP10. By extrapolating the intensity of the XPS signals of interest, i.e. Al2p, C1s, O1s, and Si2p, at each step, the depth profile was reconstructed as a function of the time of etching as shown in Figure S4b. To obtain information on the depth distribution of the inorganic infiltration inside the polymeric matrix or nanostructured domains, the time of etching was converted to a depth of etching (Figure S4c). This was done by using the effective etch rate referred to as the particular composite concentration measured at the surface before each etching step. Before each etching step, the XPS spectra reveal the relative concentration c_i of the i^{th} element on the exposed surface, i.e. C, Si, and Al, expressed in decimal atomic percent (at.%). These concentrations are used to weigh the nominal etch rates r_i of the corresponding materials, i.e. PMMA, silicon, and Al_2O_3, to find the effective etch rate. The thickness of composite material etched in the subsequent etching step is obtained by simply multiplying the effective etch rate by the time interval Δt. The obtained values are recursively summed, incrementing the depth values on the x-axis, as reported in equation S1.

$$(S1)\ d_j = d_{j-1} + \left(\sum_i c_i \cdot r_i\right)_{j-1} \cdot \Delta t$$

where d_j stands for depth of etching reached after the j^{th} etching step.

The nominal etching rates are either tabulated in the conditions of the plasma etching (Ar^+ 2 kV) or were derived from the etching of a reference material in the case of polymers. The used nominal etch rates are reported in Table S1 and carry a relative uncertainty δr of 20 %.

	PMMA	RCP/BCP	Al_2O_3	Si
Nominal etch rate r_i (nm/min)	12.4 ± 2.5	9.5 ± 1.9	4.3 ± 0.9	9.0 ± 1.8

Table S1. Nominal etch rate values for the different materials constituting the composite inorganic-organic matrix in the condition used for the plasma etching depth profiling.

The relative uncertainties on the atomic percent concentration δc are evaluated for each signal on each sample considering the signal variability and are reported in Table S2. These values are solely contributing to the uncertainty on the elemental atomic percent, reported in the depth profiles in Figure S3c and Figure 4 as the filled area around the curves.

	$\delta c_{(C1s)}$	$\delta c_{(O1s)}$	$\delta c_{(Si2p)}$	$\delta c_{(Al2p)}$
BCP10	2.8 %	2.8 %	3.0 %	1.6 %
RCP10	2.2 %	2.4 %	2.5 %	1.3 %
PMMA10	2.5 %	2.5 %	2.7 %	2.0 %

Table S2. Relative uncertainty on the atomic percent concentration for each element of interest and on each probed sample.

The uncertainty on the depth of etching, reported in Figure 4 as horizontal error bars in the Al2p and C1s curves, was obtained by standard propagation of the uncertainties δr and δc.

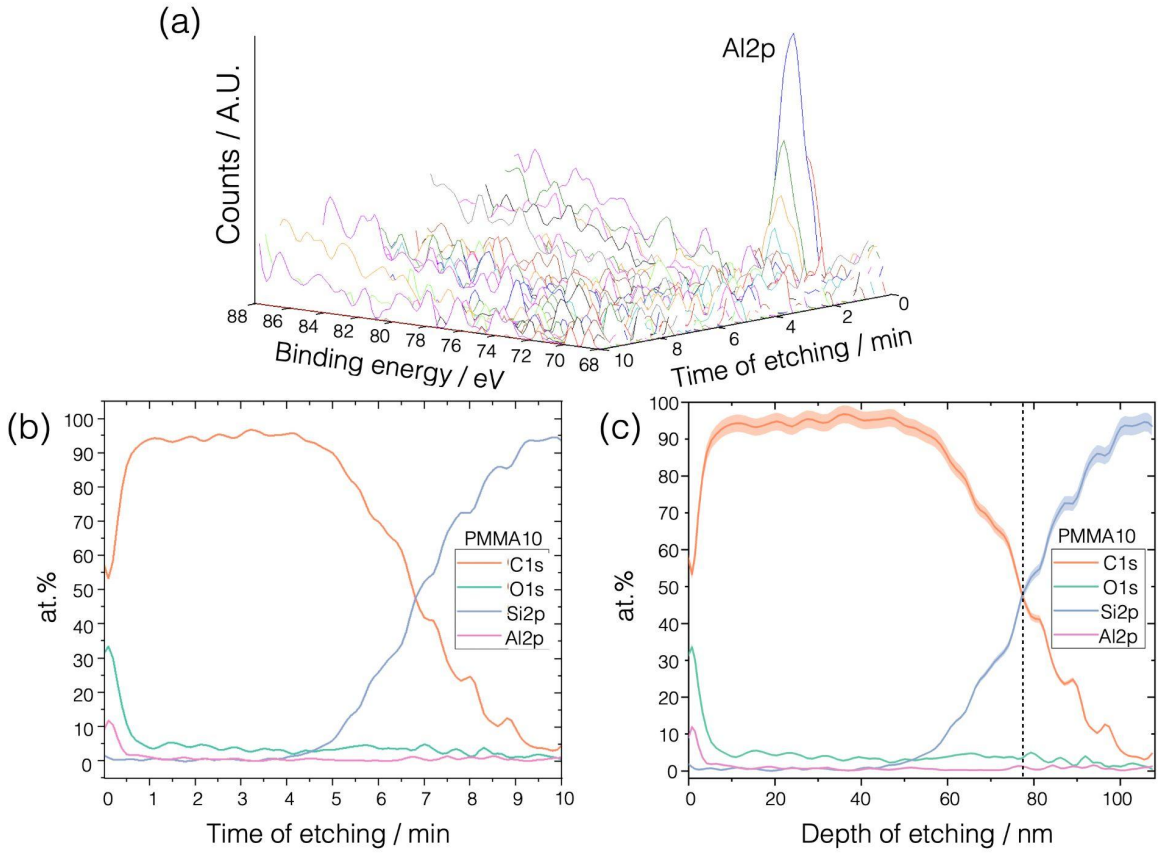

Figure S4. (a) XPS spectra were acquired on PMMA in 100 etching steps. The binding energy region around the Al2p signal is monitored and the atomic percent values are reported (b) against the time of etching to reconstruct the in-depth atomic distribution inside the composite polymer matrix. (c) The time of etching is converted to the depth of etching by using the formula in equation S1 and the inorganic depth profile inside the polymer is reported. The vertical dashed line indicates the surface of the silicon substrate. The full depth of the etching process on the PMMA10 sample is reported in this graph, while a narrower range of depths is reported in Figure 4 in the manuscript. The same conversion of the x-axis is done for the BCP10 and RCP10 samples.

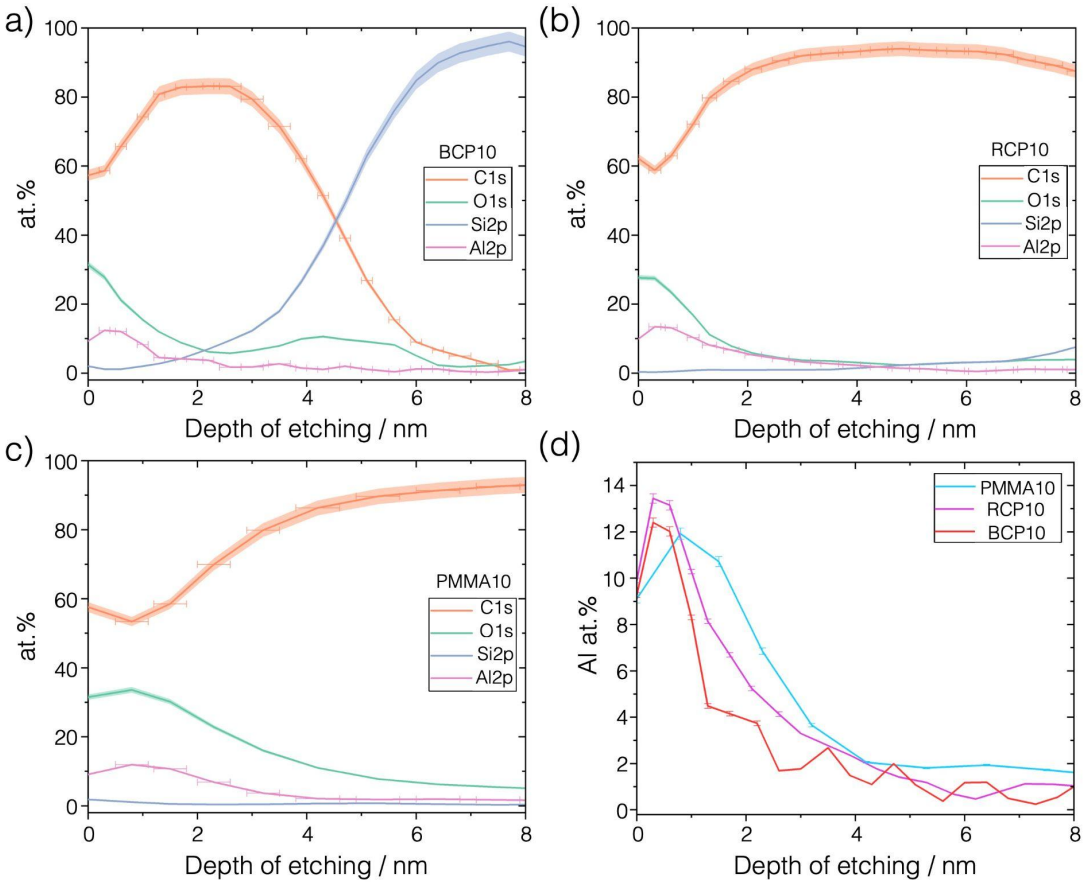

Figure S5. XPS depth profiles from Figure 4 are reported here by keeping the range of depth fixed in the interval from 0 to 8 nm to allow a more direct comparison among the different samples (a) BCP10, (b) RCP10, and (c) PMMA10. (d) The comparison of the sole aluminum curves is reported in the same depth range for the three investigated samples. It should be noted that the depth of Al in PMMA10 is the shallowest with respect to the polymer layer thickness.

EDX depth profiling

From the EDX chemical maps, the aluminum depth profiles were extracted for the three analyzed samples and the three curves are reported in the same depth range in Figure S6. With respect to the XPS depth profiles for aluminum reported in Figure S5d, it is possible to observe a relevant agreement in terms of the aluminum spatial distribution, i.e. both for PMMA10 and BCP10 the atomic concentration decays to half its initial value within the same depth range. The RCP10 distribution is slightly more broadened than its XPS counterpart. On the other hand, the atomic percent values are in modest agreement, but not precisely matched. Three facts might be considered for accounting for this quantitative difference. EDX counts, then converted to elemental concentration (at. %), are dependent on the thickness of the TEM lamella in the area of investigation, so that diverse lamellar thicknesses might result in altered concentrations. A second consideration involves the FIB micromachining of the cross-sectional TEM lamella, during the thinning of the lamella some material might be sputtered and redeposited elsewhere on the sample, leading to cross-contamination effects. A third possibility is fast carbon contamination during STEM-EDX mapping which might result in modest modification of the atomic percent values.

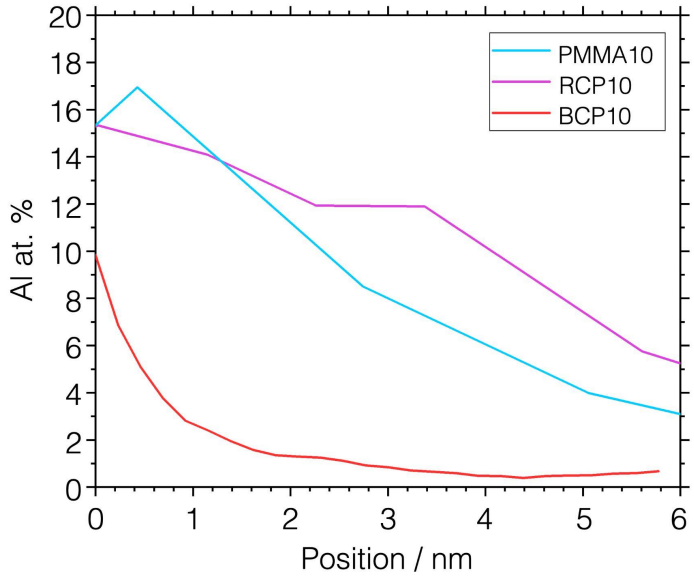

Figure S6. EDX depth profiles for aluminum are extracted from the chemical maps acquired on the three analyzed samples PMMA10, RCP10, and BCP10.